Atomic Force Microscopy of Insulin Single Crystals: Direct Visualization of Molecules and Crystal Growth

Christopher M. Yip and Michael D. Ward
Department of Chemical Engineering and Materials Science, University of Minnesota, Minneapolis, Minnesota 55455 USA

ABSTRACT Atomic force microscopy performed on single crystals of three different polymorphs of bovine insulin revealed molecularly smooth (001) layers separated by steps whose heights reflect the dimensions of a single insulin hexamer. Whereas contact mode imaging caused etching that prevented molecular-scale resolution, tapping mode imaging in solution provided molecular-scale contrast that enabled determination of lattice parameters and polymorph identification while simultaneously enabling real-time examination of growth modes and assessment of crystal quality. Crystallization proceeds layer by layer, a process in which the protein molecules assemble homoepitaxially with nearly perfect orientational and translational commensurism. Tapping mode imaging also revealed insulin aggregates attached to the (001) faces, their incorporation into growing terraces, and their role in defect formation. These observations demonstrate that tapping mode imaging is ideal for real-time in situ investigation of the crystallization of soft protein crystals of relatively small proteins such as insulin, which cannot withstand the lateral shear forces exerted by the scanning probe in conventional imaging modes.

INTRODUCTION

Correlation of protein structure with biological activity relies heavily on the determination of the protein's three-dimensional structure, typically by x-ray diffraction, which can reveal protein-receptor binding site conformations and interactions that are relevant to the rational design of pharmaceuticals (De Vos et al., 1992; Günther et al., 1990; Lambert et al., 1989). However, one of the primary obstacles to protein characterization is the growth of crystals suitable for x-ray diffraction. This difficulty stems from numerous factors, including convective currents, which lead to poor crystal quality (Koszelak et al., 1995; Day and McPherson, 1992; DeLucas et al., 1986, 1989, 1991; Erdmann et al., 1989), and aggregation processes that can lead to noncrystalline solids or crystals with high defect density and irreproducible solvent contents (Matthews, 1968). Crystal purity, size, morphology, and polymorph identity are also important issues in the manufacture, ease of delivery, and bioavailability of crystals of therapeutic proteins (Byrn, 1982; Carstensen, 1977), requiring careful optimization of crystal growth conditions such as temperature, pH, concentration, and additive levels. The need to improve protein crystallization has prompted experimental investigations (Georgalis et al., 1993; Sazaki et al., 1993; Thibault et al., 1992; Auersch et al., 1991; Kam et al., 1978; Durbin and Feher, 1990) and modeling of the nucleation and growth of protein crystals aimed toward understanding critical nuclei dimensions, relative rates of nucleation and growth, macromolecular aggregation, and the attachment of single protein molecules and their aggregates to growing crystals (Oosawa and Kasai, 1962; Noever, 1995a,b). These issues become particularly important in therapeutically important proteins such as insulin (M_r = 5.8 kDa), the hormone responsible for regulating glucose metabolism. The absence of this hormone leads to diabetes, a disease that affects approximately 1 out of every 10 persons in North America. First crystallized in 1925 (Abel and Geiling, 1925; Abel et al., 1925, 1927; Abel, 1926), insulin single crystals consist of ordered arrangements of hexamers assembled from three insulin dimers. The bioavailability and efficacy of microcrystalline insulin medications depend upon the crystal dissolution rate, which can be influenced by crystal polymorphism, morphology, and size, and the stability of the hexamer toward dissociation to active monomer form (Hollenberg, 1990; Gammeltoft, 1988; Berson and Yalow, 1966; Smith et al., 1984). Optimization of insulin crystallization would be aided significantly by direct, real-time visualization of nucleation and growth, particularly with regard to observing critical nucleation events, examining the role of aggregates and defects, identifying polymorphs, assigning actively growing crystal faces, and determining crystal quality under process conditions. These needs prompted us to examine insulin nucleation and growth by real-time in situ atomic force microscopy (AFM), which has been used successfully to examine the nucleation and growth of a variety of soft organic (Hillier and Ward, 1994; Hillier et al., 1994; Carter et al., 1994) and protein crystals (Land et al., 1995; Malkin et al., 1995; Konnert et al., 1994; Durbin et al., 1993; Durbin and Carlson, 1992).

Received for publication 16 February 1996 and in final form 5 April 1996.
Address reprint requests to Dr. Michael D. Ward, Department of Chemical Engineering and Materials Science, University of Minnesota, Amundson Hall, 421 Washington Ave. SE, Minneapolis, MN 55455. Tel.: 612-625-3062; Fax: 612-626-7246; E-mail: wardx004@maroon.tc.umn.edu.

0006-3495/96/08/1071/08 $2.00

MATERIALS AND METHODS

Bovine insulin single crystals were grown using protocols provided by Dr. G. David Smith (Hauptman-Woodward Research Institute, personal communication). The R6 rhombohedral crystallization protocol is as follows. Bovine insulin (Sigma, St. Louis, MO) was dissolved in 0.02 N HCl, 0.15 M zinc acetate, and 0.20 M sodium citrate buffer. To ensure complete

dissolution, 0.75 N NaOH was added, followed by 5% phenol and 1.0 M NaCl. The solution pH was adjusted to 8.5 with 0.75 N HCl. After standing at approximately 38°C for 3 days and subsequent cooling to ambient temperature, small clear rhombohedral crystals formed after several hours.

Atomic force microscopy images were obtained on a Digital Instruments NanoScope III MultiMode scanning probe microscope. Contact mode imaging was performed with Si_3N_4 cantilevers with a measured spring constant of 0.074 $N \cdot m^{-1}$, as determined by an end-mass resonance technique (Cleveland et al., 1993). Tapping mode imaging was performed with identical cantilevers, but with oxide-sharpened tips (Digital Instruments, Santa Barbara, CA). The reported AFM images were taken using the E scanning head, which has a maximum lateral scan window of 14.6 × 14.6 μm. For imaging in air, crystals were transferred by pipette onto either a polished AFM mount coated with a small amount of spray adhesive or a small tab of freshly cleaved mica affixed to the AFM mount. The mother liquor was then quickly wicked away and the AFM tip was positioned over a suitable crystal. The regions imaged were free of macroscopic surface defects, as determined by optical microscopy. Imaging in solution was carried out in a combination contact/tapping mode liquid cell (Digital Instruments). The insulin crystals in their mother liquor were introduced into a well that was defined by an O-ring placed on an AFM mount coated with a thin layer of vacuum grease. The AFM liquid cell was carefully placed over the O-ring, and saturated mother liquor was introduced to the cell.

Tapping mode imaging in solution was performed at cantilever drive frequencies ranging from 6 kHz to 32 kHz. Viscous coupling between the cantilever and the fluid results in a number of broad resonant peaks, and therefore, the choice of an appropriate drive frequency cannot be determined a priori. The cantilever drive and setpoint voltages, which determine the cantilever oscillation magnitude to be controlled by the feedback circuit during imaging, have a dramatic effect on image quality. These parameters are chosen in each experiment such that image quality is optimized with respect to resolution, contrast, and sample integrity. Increasing the setpoint voltage in tapping mode corresponds to increasing the average sample-tip separation. Small increases (typically ~0.03 V) in the setpoint voltage from an optimized value during insulin imaging results in deterioration of image quality due to tip disengagement and diminished resolution. Based on the aforementioned cantilever spring constant and the cantilever-photodiode sensitivity, this suggests that the imaging force is approximately 100 pN during imaging, in qualitative agreement with previous reports (Radmacher et al., 1994). The optimum cantilever drive and setpoint voltages will depend strongly on the cantilever spring constant, drive frequency, and coupling between the tip and surrounding fluid. It should also be noted that a similar decrease in setpoint voltage from an optimized value results in mechanical etching of the sample. Image analyses were performed on low-pass filtered AFM data using Nanoscope III, version 4.21b2 (Digital Instruments) and National Institutes of Health Image version 1.59 (National Institutes of Health; available by anonymous file transfer protocol from zippy.nimh.nih.gov) software packages.

RESULTS

AFM images of the (001) faces of the R6 rhombohedral, T6 rhombohedral, and R6 monoclinic polymorphs of bovine insulin, acquired in conventional contact mode directly in mother liquor, revealed molecularly smooth terraces with micron-scale lateral dimensions (Fig. 1). The heights of the steps separating the terraces were 43 Å and 50 Å for the rhombohedral and monoclinic forms. (The AFM data for the T6 rhombohedral form are indistinguishable from that of the R6 rhombohedral form and therefore are not reported in detail here.) These heights were consistent with the *c*-axis dimensions of these forms (Baker et al., 1988; Derewenda et al., 1989; Smith and Ciszak, 1995; Smith and Dodson, 1992; Ciszak and Smith, 1994; Kaarsholm et al., 1989; R6

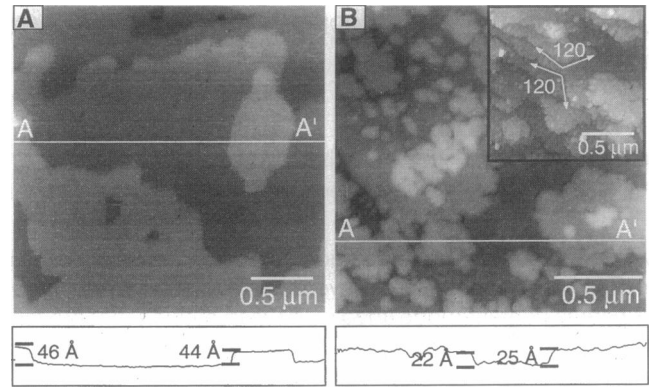

FIGURE 1 (*A*) Contact mode AFM image revealing large molecularly flat terraces observed on the (001) face of R6 rhombohedral bovine insulin in mother liquor. Terrace heights are consistent with the *c*-axis lattice constant for this polymorph (c = 40.39 Å). Scan size: 2.5 μm × 2.5 μm. Scan rate: 5.55 Hz. (*B*) Tapping mode AFM image of the (001) face of R6 rhombohedral bovine insulin acquired in air, revealing large (~60 nm) rounded aggregates on the terraces and step edges. Narrow canyons between adjacent terraces support a small amount of lateral contraction during fracturing that accompanies crystal dehydration. Terrace heights obtained in air are consistent with the thickness of an isolated insulin hexamer unit. Scan size: 2.5 μm × 2.5 μm. Scan rate: 4.60 Hz. (*Inset*) Terrace and ledges of T6 rhombohedral polymorph imaged in air under tapping mode conditions. The steps are scalloped and have well-defined 120° angles, consistent with (hk0) step planes, most likely (110). Inset scan size: 1.25 μm × 1.25 μm. Scan rate: 12 Hz. Height profiles are taken along lines marked A-A′.

rhombohedral: space group R3, $a = b$ = 79.92 Å, c = 40.39 Å as indexed on hexagonal axes; R6 monoclinic: $P2_1$ space group with lattice parameters a = 61.23 Å, b = 61.65 Å, c = 48.05 Å, β = 110.50°; G. D. Smith, personal communication). These values are in good agreement with the estimated thickness of an isolated insulin hexamer, which has been described as an oblate spheroid with a diameter of approximately 50 Å and a height of 35 Å (Blundell et al., 1972). In contrast, AFM images acquired in air using contact and tapping mode revealed terraces separated by steps with heights ranging from 23 Å to 29 Å. The smaller heights in air are attributed to dehydration of the (001) protein layers upon removal of the crystals from solution. The observed decrease in the thickness of the (001) layers upon dehydration corresponds to a ~40% volume change when shrinkage is assumed to be along the *c*-axis and is in good agreement with the estimated 30–35% solvent content for these polymorphs (G. D. Smith, personal communication; Gursky et al., 1992; Badger and Casper, 1991; Dodson et al., 1978). The hydrated and dehydrated surfaces also differ with respect to the integrity and roughness of the terraces, which fracture upon dehydration, and the viscoelastic response of the surface protein layers to applied tip forces (Yip and Ward, manuscript in preparation).

Despite small imaging forces estimated at 30 nN and 4 nN in air and solution, respectively, all attempts to obtain molecular-scale contrast of the (001) layers using contact mode in air and solution were thwarted by etching of these

surfaces. However, the (001) surfaces were mechanically robust toward tapping mode imaging performed in solution (Hansma et al., 1994). This imaging mode measures changes in the amplitude of an oscillating cantilever tip and minimizes the contact and lateral forces between the tip and the sample. Furthermore, solution imaging eliminates capillary forces and, in appropriate solvents, reduces attractive weaker van der Waals forces between the tip and sample (Hutter and Bechhoefer, 1993). The effective loading forces exerted during tapping mode imaging cannot be measured directly but have been estimated to be below 200 pN (Radmacher et al., 1994). These effects make tapping mode in solution an ideal approach for investigating very soft materials, as recently demonstrated by observations of isolated protein molecules on mica (Fritz et al., 1995).

The stability of the (001) layers during tapping mode enabled the observation of contrast attributable to ordered insulin hexamers in the (001) planes of these polymorphs (Fig. 2). In the case of the R6 rhombohedral polymorph, the molecular-scale real and Fourier space AFM data acquired for the (001) layers conformed to a hexagonal cell with a lattice dimension of 42.8 ± 6.4 Å, in agreement with the 45.65 Å spacing of hexagonally packed, nearest-neighbor insulin hexamers along the [1$\bar{1}$0] and [120] directions, as calculated from the single crystal x-ray structure. Similarly, the molecular-scale real and Fourier space data acquired for the (001) face of the R6 monoclinic polymorph clearly revealed a nearly square lattice, consistent with the symmetry of the (001) plane of this polymorph. Furthermore, the dimension of this lattice was 45.8 Å ± 1.0 Å, in good agreement with the nearest-neighbor contacts along [110] and [1$\bar{1}$0] on the (001) face. The AFM unit cells, deduced from the Fourier spectra, are equivalent alternative descriptions of the unit cells chosen for single-crystal x-ray diffraction structure solution. Comparison of the molecular-scale contrast on (001) terraces separated by single steps revealed that the protein layers were rotationally and translationally commensurate, to within 4° and 5 Å for these polymorphs (these values are comparable to the experimental error). This high degree of commensurism during homoepitaxial growth is illustrative of good crystal quality with respect to ordering of the (001) layers, which is critical for diffraction analysis. Furthermore, the layer stacking deduced from data acquired on consecutive terraces is consistent with the space groups of the respective forms, which do not have close-packed layer stacking (Wilson, 1992). These data demonstrate that AFM can be used to confirm space group symmetries, determine lattice parameters, and identify polymorphs, thereby providing rudimentary crystallographic data for crystals too small for single-crystal diffraction measurements.

It is noteworthy that molecular-scale contrast has been observed in contact mode AFM studies of canavalin (Mr = 147 kDa) and cubic satellite tobacco mosaic virus (Mr = 1450 kDa) in which the crystal lattice contains layers of proteins (Land et al., 1995; Malkin et al., 1995). Apparently, insulin is susceptible to damage by the lateral shear forces exerted by the AFM tip during contact mode imaging, suggesting that tapping mode imaging is the method of choice for this system. Although molecular-scale contrast generally is not observed with tapping mode, owing to its poorer inherent resolution compared to contact mode, the achievement of molecular-scale contrast here can be attributed partly to the large lattice constants of the (001) layer.

Tapping mode imaging in solution below supersaturation revealed small aggregates on the (001) layers of all three polymorphs. These aggregates, illustrated in Fig. 3 *A* for the R6 rhombohedral polymorph, were oriented along the [$\bar{1}$10] direction and were stable indefinitely during tapping mode imaging at concentrations below supersaturation. Their morphology and shape orientation were independent of scan orientation. The aggregates appear to be composed of multiples of poorly defined ellipsoids with average lateral dimensions of 110 Å × 52 Å and a nominal height of 28 Å. This size, although possibly inaccurate because of tip effects, is roughly equivalent to two insulin hexamers. Based on the solution aggregation behavior of insulin, it seems likely that these features reflect the attachment of precrystallization aggregates formed in solution (Milthorpe et al., 1977; Bohinder and Geissler, 1984; Pederson et al., 1994; Jeffrey, 1974; Hvidt, 1991). Similar behavior has been reported for other proteins (Wilson and Pusey, 1992; Pusey, 1991; Ataka and Asai, 1990; Durbin and Carlson, 1992; Sazaki et al., 1993; Kadima et al., 1990), and theoretical models of protein attachment kinetics have suggested that aggregate addition has at least the same probability as that for individual monomer units. Furthermore, the probability of multiple binding sites compensates for the decreased diffusivity of the larger aggregates (Noever, 1995a,b).

If the solution was allowed to achieve slight supersaturation by simply allowing a small amount of water to evaporate from a saturated solution, layer-by-layer growth commenced in which (001) terraces grew by step flow across the image frame (Fig. 4). Under these conditions, the terraces on the insulin (001) face generally had areas exceeding 10 μm^2, with relatively few steps. This suggests that the (001) face has a relatively low surface energy and that attachment to the steps is thermodynamically preferred over two-dimensional nucleation. The growth rate under these conditions was approximately 10^4 $nm^2 \cdot s^{-1}$ in terms of terrace growth and ~5 $nm \cdot s^{-1}$ in terms of advancement of the growth front. The growth rates were calculated by comparison to the location of stationary defects that served as landmarks. Careful examination of time lapse images indicates that growth is fastest along the [110], [1$\bar{1}$0], and [120] directions for the rhombohedral forms and along the [110] and [1$\bar{1}$0] directions for the R6 monoclinic form. These directions represent the closest contact between insulin hexamers and, accordingly, would be expected to be the fast growth directions. Assuming crystal growth occurs at the saturated concentration, measurements of local radius of curvature at multiple points along the larger growing step edges (~131 ± 59 nm), suggested that the free energy of a unit step edge, α, was approximately 3×10^{-7} $J \cdot cm^2$ with

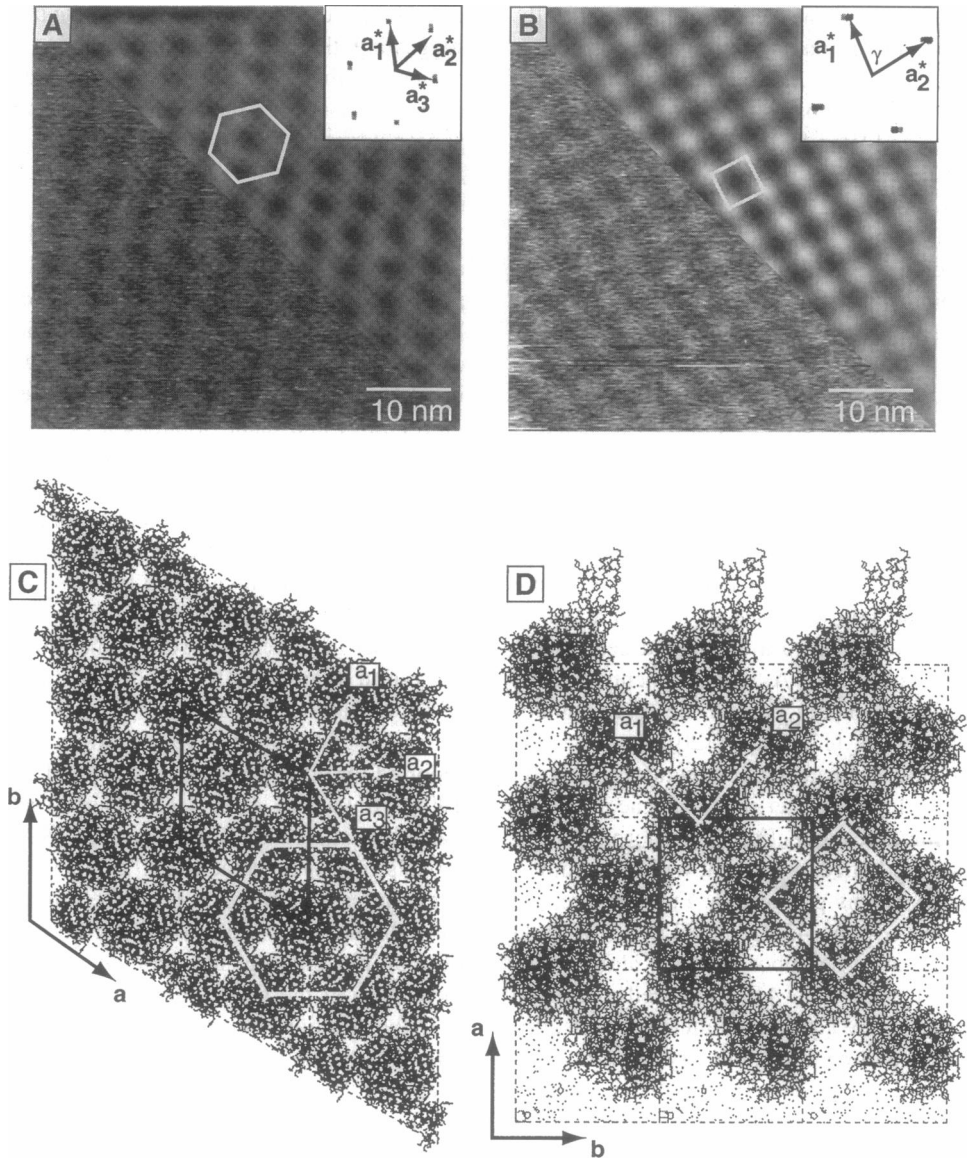

FIGURE 2 (*A*) Raw and Fourier-filtered real space data for the (001) face of the R6 rhombohedral polymorph of bovine insulin. Scan size: 50 nm × 50 nm. Scan rate: 5.55 Hz. (*Inset*) Two-dimensional Fourier power spectrum revealing reciprocal lattice vectors corresponding to real space periodicities of $a_1 = 41.5$ Å; $a_2 = 37.2$ Å; $a_3 = 49.8$ Å; $\gamma_{12} = 47°$; $\gamma_{23} = 54°$. The slight distortion from hexagonal symmetry is attributed to scanning artifacts. (*B*) Raw and Fourier-filtered real space data for the (001) face of the R6 monoclinic polymorph of bovine insulin. (*Inset*) Two-dimensional Fourier power spectrum revealing reciprocal lattice vectors corresponding to real space periodicities of $a_1 = 46.4$ Å; $a_2 = 45.1$ Å; $\gamma_{12} = 84°$. Scan size: 50 nm × 50 nm. Scan rate: 8.14 Hz. (*C*) Insulin hexamer packing motif of the (001) face of the R6 rhombohedral polymorph of bovine insulin based on single crystal x-ray diffraction data. The real space vectors a_1, a_2, and a_3 correspond to the nearest-neighbor hexamer vectors [120], [210], [1$\bar{1}$0], respectively. (*D*) Insulin hexamer packing motif of the (001) face of the R6 monoclinic polymorph of bovine insulin based on single crystal x-ray diffraction data. The real space vectors a_1 and a_2 correspond to the nearest-neighbor hexamer vectors [110] and [1$\bar{1}$0], respectively. Unit cells based on single crystal x-ray diffraction data are shown as solid black lines. The R6 rhombohedral polymorph crystallizes in space group R3 with lattice parameters $a = b = 79.92$ Å, $c = 40.39$ Å indexed on hexagonal axes. The R6 monoclinic polymorph crystallizes in space group $P2_1$ with lattice parameters $a = 61.23$ Å, $b = 61.65$ Å, $c = 48.05$ Å, $\beta = 110.50°$. AFM unit cells corresponding to the two-dimensional Fourier power spectra are depicted as solid white lines. Note that the position of the AFM unit cells in the *x-y* plane is arbitrary. The AFM unit cells, deduced from the Fourier spectra, are equivalent alternative descriptions of the unit cells chosen for single crystal x-ray diffraction structure solution. Structural models were prepared with Cerius^2, version 1.6 (BIOSYM/Molecular Simulations Inc., San Diego, CA).

a corresponding kinetic growth coefficient, β, of 10^{-3}-10^{-4} cm·s^{-1} (Burton et al., 1951). These values are comparable to those determined from recent AFM studies of canavalin and satellite tobacco mosaic virus crystal growth (Land et al., 1995; Malkin et al., 1995), but are approximately two orders of magnitude smaller than those determined for inorganic systems (Söhnel, 1982). The small α value is most likely due to the large solvent content of the proteins, which minimizes the difference between the step surface energy and the protein in solution. The small β value may reflect

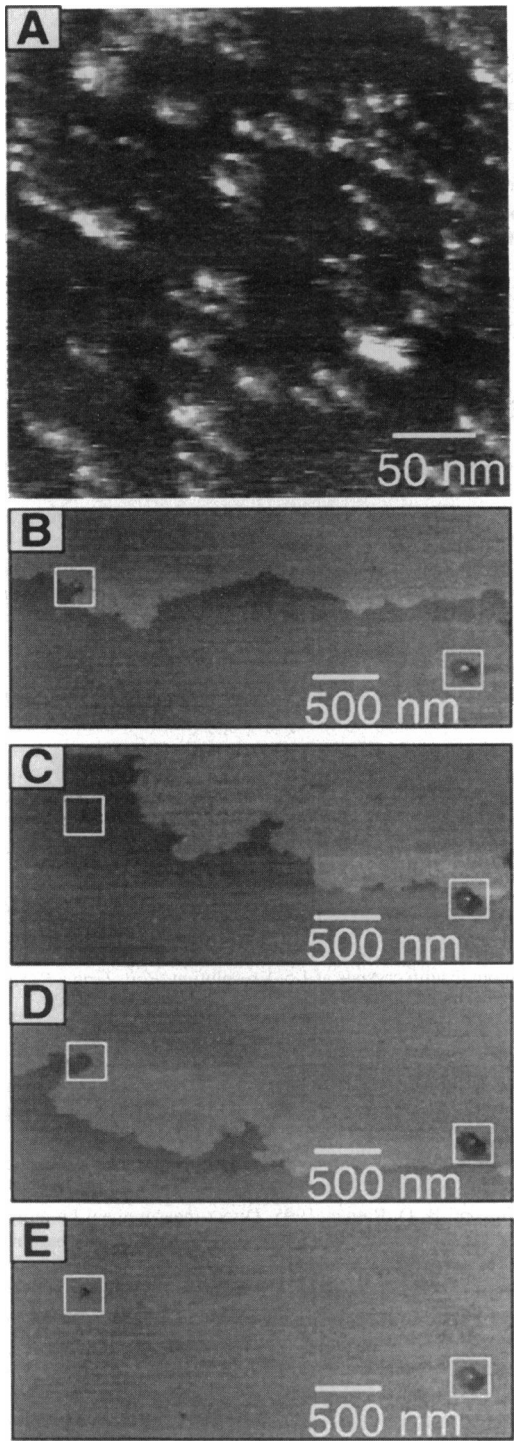

FIGURE 3 (*A*) In situ AFM tapping mode image of protein aggregation on the (001) face of the R6 rhombohedral polymorph of bovine insulin. The aggregates appear to be oriented along the [1$\bar{1}$0] direction, as deduced from comparison to the molecular-scale contrast of the underlying (001) crystal face. Scan size: 300 nm × 300 nm. Scan rate: 2.97 Hz. (*B–E*) Real-time in situ tapping mode images collected at 0, 643, 772, and 801 s, respectively, revealing formation of persistent core dislocations instigated by misaligned protein aggregrates. Note that one complete terrace has filled the scanning frame between images *B* and *C*. A new terrace has entered the frame in image *C* and has filled the scanning frame in image *E*. Outlines indicate the location of aggregates and core dislocations. Image size: 1.5 μm × 3.5 μm. Scan rate: 2.0 Hz.

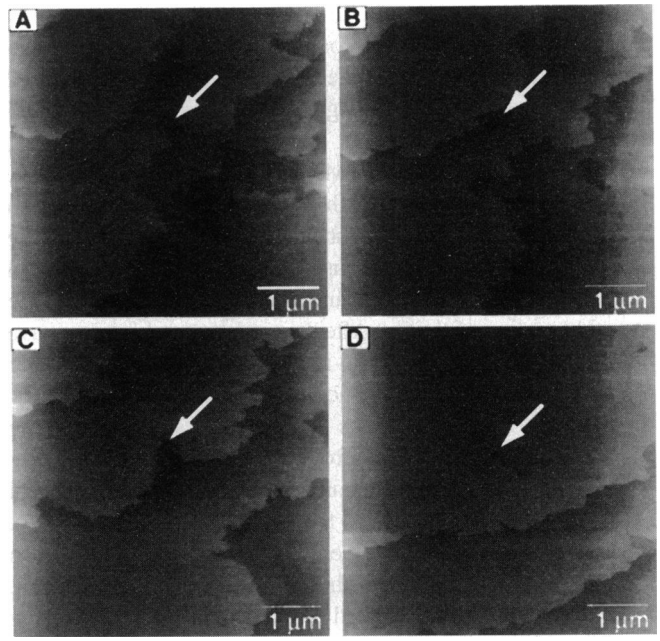

FIGURE 4 (*A–D*) Real-time in situ tapping mode images of R6 rhombohedral polymorph of bovine insulin collected at 0, 257, 644, and 1287 s, respectively, revealing layer-by-layer growth of individual insulin terraces. Scan size: 5 μm × 5 μm. Scan rate: 2.0 Hz. The arrow indicates the position of a stationary defect site used as a landmark for calculating terrace growth rates.

the difficulty in achieving the correct orientation of either single proteins or protein aggregates during attachment at the step sites, or the low diffusion coefficient for insulin ($\sim 7.9 \times 10^{-7}$ cm^2·s^{-1} (Hvidt, 1991)) or its precrystallization aggregates.

Under conditions of step growth, the aforementioned aggregates typically are consumed by the steps as they flow across the crystal surface and form new (001) layers, although we cannot determine whether the aggregates directly attach to the steps or dissociate to hexamers, dimers, or monomers, which subsequently diffuse along the surface and attach to the step. Occasionally, these aggregates formed a surface diffusion barrier to growth at the step edge, as evidenced by steps that grew around the aggregate, leaving a small hole that persists upon growth of additional (001) layers (Fig. 3 *B–E*). These holes are similar to those reported recently for lysozyme, canavalin, and satellite tobacco mosaic virus crystals (Land et al., 1995; Malkin et al., 1995; Konnert et al., 1994; Durbin et al., 1993; Durbin and Carlson, 1992). We have not observed dislocations emerging from these holes, and these features do not appear to otherwise affect the growth of the (001) terraces. However, it is likely that they occlude mother liquor, which can be deleterious for single-crystal x-ray diffraction and the physical properties of commercial formulations. These defects differ from pits introduced by intentional mechanical etching with the AFM tip, which are transient and rapidly fill in by the same layer growth mechanism described above. These observations suggest that some insulin aggregates

attached to the (001) face are strongly bound and cannot achieve the correct orientation, migrate to the step, or dissociate into more mobile species on the time scale of the terrace growth, thereby instigating the creation of dislocation cores.

Previous contact-mode AFM studies of crystal growth have indicated that apparent growth rates are faster in the region being scanned compared to surrounding regions. This may be due to defect formation caused by the tip (LaGraff and Gewirth, 1994, 1995) or enhanced convection caused by the rastering motion of the tip. After extensive searching, we have not found any evidence for tip-induced defect formation under typical scanning conditions, nor have we detected any screw dislocations that may serve as the source of steps, suggesting very low densities of these growth centers. Furthermore, we have not observed, under our conditions, two-dimensional islands such as those observed for STMV (Malkin et al, 1995). Rather, growing terraces entered the scanning frame from outer regions, indicating that the tip was not initiating growth. After the growing terrace filled the scanning frame, expanding the field of view about the original scanned region revealed that growth was somewhat faster in the scanned regions than in the outlying regions, similar to behavior reported for canavalin (Land et al., 1995). These observations suggest that a very small number of dislocations initiate the formation of steps remote from the scanning region, but that the tip enhances mixing of the boundary layer at the growing crystal surface as a consequence of its vertical and horizontal motion, thereby enhancing otherwise diffusion-limited growth.

These studies illustrate that tapping-mode AFM performed directly in solution provides resolution of molecular-scale contrast, which enables the identification of different polymorphs of bovine insulin, confirmation of the crystal packing and symmetry, and insight into the growth mechanisms. The apparent absence of screw dislocations, although the actively growing steps most likely emanate from them, indicates that insulin crystals can be grown with a minimal number of these defects. However, impurities or misaligned aggregates bound to actively growing crystal faces can instigate the formation of core dislocations. We anticipate that the ability to resolve molecular-scale contrast while simultaneously visualizing the nanoscale topography and growth modes of the morphologically important faces of insulin single crystals will become a useful approach for optimizing crystallization conditions of this therapeutically important protein and its modified forms. The capabilities of in situ AFM provide an opportunity for the direct examination of the influence of various experimental parameters during growth at the near-molecular level, instead of relying on inference from inspection of mature crystals. This includes studies aimed toward the elucidation of the role of additives in polymorph selectivity (Kaarsholm et al., 1989; Derewenda et al., 1989; Smith and Dodson, 1992; Ciszak and Smith, 1994), solid-state structure (Smith and Ciszak, 1994) and crystal morphology (Markman et al., 1992), protein-receptor interactions (Lee et al., 1994a,b; Boland and Ratner, 1995; Florin et al., 1994; Moy et al., 1994; Chilkoti et al., 1995; Ohnesorge et al., 1992; Drake et al., 1989; Weisenhorn et al., 1992), and the formation of cocrystals with other proteins (Low et al., 1974; Krayenbühl and Rosenberg, 1946; Hagedorn et al., 1936).

We gratefully acknowledge the assistance of Dr. Cecil C. Yip (University of Toronto), Dr. G. David Smith (Hauptman-Woodward Research Institute), Ms. Nikki Dahlin (University of Minnesota), and Mr. Erik M. Jerde (University of Minnesota).

We acknowledge the National Science Foundation for financial support and the Office of Naval Research for equipment.

REFERENCES

Abel, J. J. 1926. Crystalline insulin. *Proc. Natl. Acad. Sci. USA.* 12: 132–136.

Abel, J. J., and E. M. K. Geiling. 1925. Researches on insulin. I. Is insulin an unstable sulphur compound? *J. Pharmacol. Exp. Ther.* 25:423–448.

Abel, J. J., E. M. K. Geiling, G. Alles, and A. Raymond. 1925. Researches on insulin. I. Is insulin an unstable sulphur compound? *Science.* 47: 169–171.

Abel, J. J., E. M. K. Geiling, O. A. Roultier, F. M. Bell, and O. Wintersteiner. 1927. Crystalline insulin. *J. Pharmacol. Exp. Ther.* 31:65–85.

Ataka, M., and M. Asai. 1990. Analysis of the nucleation and crystal growth kinetics of lysoyme by a theory of self-assembly. *Biophys. J.* 58:807–811.

Auersch, A., W. Littke, P. Lang, and W. Burchand. 1991. Static and dynamic light scattering on solutions of precrystalline beta-galactosidase. *J. Crystal Growth.* 110:201–207.

Badger, J., and D. L. D. Caspar. 1991. Water structure in cubic insulin crystals. *Proc. Natl. Acad. Sci. USA.* 88:622–626.

Baker, E. N., T. J. Blundell, J. F. Cutfield, S. M. Cutfield, E. J. Dodson, G. G. Dodson, D. C. Hodgkin, R. E. Hubbard, N. W. Isaacs, C. D. Reynolds, K. Sakabe, N. Sakabe, and N. M. Vijayan. 1988. The structure of 2Zn pig insulin crystals at 1.5 Å resolution. *Phil. Trans. R. Soc. Lond.* 319:369–456.

Berson, S. A., and R. S. Yalow. 1966. Insulin in blood and insulin antibodies. *Am. J. Med.* 40:676–690.

Blundell, T., G. Dodson, D. Hodgkin, and D. Mercola. 1972. Insulin: the structure in the crystal and its reflection in chemistry and biology. *Adv. Protein Chem.* 26:280–402.

Bohindar, H. B., and E. Geissler. 1984. Static and dynamic light scattering from dilute insulin solutions. *Biopolymers.* 23:2407–2417.

Boland, T., and B. D. Ratner. 1995. Direct measurement by atomic force microscopy of hydrogen bonding in DNA nucleotide bases. *Proc. Natl. Acad. Sci. USA.* 92:5297–5301.

Burton, W. K., N. Cabrera, and F. C. Frank. 1951. The growth of crystals and the equilibrium structure of their surfaces. *Phil. Trans. R. Soc. Lond. A.* 243:299–358.

Byrn, S. R. 1982. Solid-State Chemistry of Drugs. Academic Press, New York.

Carstensen, J. T. 1977. Pharmaceutics of Solids and Solid Dosage Forms. John Wiley and Sons, New York.

Carter, P. W., A. C. Hillier, and M. D. Ward. 1994. Nanoscale surface topography and growth of molecular crystals: the role of anisotropic intermolecular bonding. *J. Am. Chem. Soc.* 116:944–953.

Chilkoti, A., T. Boland, T., B. D. Ratner, and P. S. Stayton. 1995. The relationship between ligand-binding thermodynamics and protein-ligand interaction forces measured by atomic force microscopy. *Biophys. J.* 69:2125–2130.

Ciszak, E., and G. D. Smith. 1994. Crystallographic evidence for dual coordination around zinc in the T_3R_3 human insulin hexamer. *Biochemistry.* 33:1512–1517.

Cleveland, J. P., S. Manne, D. Bocek, and P. K. Hansma. 1993. A nondestructive mthod for determining the spring constant of cantilevers for scanning force microscopy. *Rev. Sci. Instrum.* 64:403–405.

Day, J., and A. McPherson. 1992. Macromolecular crystal growth experiments on International Microgravity Laboratory-1. *Protein Sci.* 1:1254–1568.

Delucas, L. J., C. D. Smith, H. W. Smith, V.-K. Senadhi, S. E. Senadhi, S. E. Ealick, C. E. Bugg, D. C. Carter, R. S. Snyder, P. C. Weber, F. R. Salemme, D. H. Ohlendorf, H. M. Einspahr, L. L. Clancey, M. A. Navia, B. M. McKeever, T. L. Nagabhushan, G. Nelson, Y. S. Babu, A. McPherson, S. Koszelak, D. Stammers, K. Powell, and G. Darby. 1989. Protein crystal growth in microgravity. *Science.* 246:651–654.

Delucas, L. J., C. D. Smith, H. W. Smith, V.-K. Senadhi, S. E. Senadhi, S. E. Ealick, D. C. Carter, R. S. Snyder, P. C. Weber, F. R. Salemme, D. H. Ohlendorf, H. M. Einspahr, L. L. Clancey, M. A. Navia, B. M. McKeever, T. L. Nagabhushan, G. Nelson, A. McPherson, S. Koszelak, G. Taylor, D. Stammers, K. Powell, G. Darby, and C. E. Bugg. 1991. Protein crystal gowth results for shuttle flights STS-26 and STS-29. *J. Crystal Growth.* 110:302–311.

Delucas, L. J., F. L. Suddath, R. Snyder, R. Naumann, M. B. Broom, M. Pusey, V. Yost, B. Herren, D. Carter, B. Nelson, E. J. Meehan, A. McPherson, and C. E. Bugg. 1986. Preliminary investigations of protein crystal growth using the space shuttle. *J. Crystal Growth.* 76:681–693.

Derewenda, U., Z. Derewenda, E. J. Dodson, G. G. Dodson, C. D. Reynolds, G. D. Smith, C. Sparks, and D. Swenson. 1989. Phenol stabilizes more helix in a new symmetrical zinc insulin hexamer. *Nature.* 338:594–596.

De Vos, A. M., M. Ultsch, and A. A. Kossiakoff. 1992. Human growth hormone and extracellular domain of its receptor: crystal structure of the complex. *Science.* 255:306–312.

Dodson, E. J., G. G. Dodson, A. Lewitova, and M. Sabesan. 1978. Zinc-free cubic pig insulin: crystallization and structure determination. *J. Mol. Biol.* 125:387–396.

Drake, B., C. B. Prater, A. L. Weisenhorn, S. A. C. Gould, T. R. Albrecht, C. F. Quate, D. S. Cannell, H. G. Hansma, and P. K. Hansma. 1989. Imaging crystals, polymers and processes in water with the atomic force microscope. *Science.* 243:1586–1589.

Durbin, S. D., and W. E. Carlson. 1992. Lysozyme crystal growth studied by atomic force microscopy. *J. Crystal Growth.* 122:71–79.

Durbin, S. D., W. E. Carlson, and M. T. Saros. 1993. In situ studies of protein crystal growth by atomic force microscopy. *J. Phys. D. Appl. Phys.* 26:B128–B132.

Durbin, S. D., and G. Feher. 1990. Studies of crystal growth mechanisms of proteins by electron microscopy. *J. Mol. Biol.* 212:763–774.

Erdmann, V. A., C. Lippmann, C. Betzel, Z. Dauter, K. Wilson, R. Hilgenfeld, J. Hoven, A. Liesum, W. Saenger, A. Muller-Fahrnow, W. Hinrichs, M. Duvel, G. Schulz, C. W. Muller, H. G. Wittmann, A. Yonath, G. Weber, K. Stegen, and A. Plaas-Link. 1989. Crystallization of proteins under microgravity. *FEBS Lett.* 259:194–198.

Florin, E-L., V. T. Moy, and H. E. Gaub. 1994. Adhesion forces between individual ligand-receptor pairs. *Science.* 264:415–417.

Fritz, M., M. Radmacher, J. P. Cleveland, M. R. Allersma, R. J. Stewart, R. Gieselmann, P. Janmey, C. F. Schmidt, and P. K. Hansma. 1995. Imaging globular and filamentous proteins in physiological buffer solutions with tapping mode atomic force microscopy. *Langmuir.* 11: 3529–3535.

Gammeltoft, S. 1988. Insulin Receptors. Part A: Methods for the Study of Structure and Function. Allan R. Liss, New York.

Georgalis, Y., A. Zouni, W. Eberstein, and W. Saenger. 1993. Formation dynamics of protein precrystallization fractal clusters. *J. Crystallogr. Growth.* 126:245–260.

Günther, N., C. Betzel, and W. Weber. 1990. The secreted form of the epidermal growth factor receptor. Characterization and crystallization of the receptor-ligand complex. *J. Biol. Chem.* 265:22082–22085.

Gursky, O., J. Badger, Y. Li, and D. L. D. Caspar. 1992. Conformational changes in cubic insulin crystals in the pH range 7–11. *Biophys. J.* 63:1210–1220.

Hagedorn, H. C., B. N. Jensen, N. B. Krarup, and I. Woodstrup. 1936. Protamine insulin. *JAMA.* 106:177–180.

Hansma, P. K., J. P. Cleveland, M. Radmacher, D. A. Walters, P. E. Hillner, M. Bezanilla, M. Fritz, D. Vie, H. G. Hansma, C. R. Prater, J. Massie, L. Fukunaga, J. Gurley, and V. Elings. 1994. Tapping mode atomic force microscopy in liquids. *Appl. Phys. Lett.* 64:1738–1740.

Hillier, A. C., J. B. Maxson, and M. D. Ward. 1994. Electrocrystallization of an ordered organic monolayer: selective epitaxial growth of β-$(ET)_2I_3$ on graphite. *Chem. Mater.* 6:2222–2226.

Hillier, A. C., and M. D. Ward. 1994. Atomic force microscopy of the electrochemical nucleation and growth of molecular crystals. *Science.* 263:1261–1264.

Hollenberg, M. D. 1990. Receptor triggering and receptor regulation: structure-activity relationships from the receptor's point of view. *J. Med. Chem.* 33:1275–1281.

Hutter, J. L., and J. Bechhoefer. 1993. Manipulation of van der Waals forces to improve image resolution in atomic-force microscopy. *J. Appl. Physiol.* 73:4123–4129.

Hvidt, S. 1991. Insulin association in neutral solution studied by light scattering. *Biophys. Chem.* 39:205–213.

Jeffrey, P. D. 1974. Polymerization behavior of bovine-zinc insulin at neutral pH. Molecular weight of the subunit and the effect of glucose. *Biochemistry.* 13:4441–4447.

Kaarsholm, N. C., H-C. Ko, and M. F. Dunn. 1989. Comparison of solution structural flexibility and zinc binding domains for insulin, proinsulin and miniproinsulin. *Biochemistry.* 28:4427–4435.

Kadima, W., A. McPherson, M. F. Dunn, and F. A. Jurnak. 1990. Characterization of precrystallization aggregation of canavalin by dynamic light scattering. *Biophys. J.* 57:125–132.

Kam, Z., H. B. Shore, and G. Feher. 1978. On the crystallization of proteins. *J. Mol. Biol.* 123:539–555.

Konnert, J. H., P. D'Antonio, and K. B. Ward. 1994. Observations of growth steps, spiral dislocations and molecular packing on the surface of lysozyme crystals with the atomic force microscope. *Acta. Crystallogr.* D50:603–613.

Koszelak, S., J. Day, C. Leja, R. Cudney, and A. McPherson. 1995. Protein and virus crystal growth on International Microgravity Laboratory-2. *Biophys. J.* 69:13–19.

Krayenbühl, C., and T. Rosenberg. 1946. Crystalline protamine insulin. *Rep. Steno. Hosp. (Kbh.).* 1:60–73.

Lambert, G., E. A. Stura, and I. A. Wilson. 1989. Crystallization and preliminary X- ray diffraction studies of a complex between interleukin-2 and a soluble form of the p55 component of the high affinity interleukin-2 receptor. *J. Biol. Chem.* 264:12730–12736.

LaGraff, J. R., and A. A. Gewirth. 1994. Enhanced electrochemical deposition with an atomic force microscope. *J. Phys. Chem.* 98: 11246–11250.

LaGraff, J. R., and A. A. Gewirth. 1995. Nanometer-scale mechanism for the constructive modification of Cu single crystals and alkanethiol passivated Au(111) with an atomic force microscope. *J. Phys. Chem.* 99:10009–10018.

Land, T. J., A. J. Malkin, Y. G. Kuznetsov, A. McPherson, and J. J. De Yoreo. 1995. Mechanisms of protein crystal growth: an atomic force microscopy study of canavalin crystallization. *Phys. Rev. Lett.* 75: 2774–2777.

Lee, G. U., L. A. Chrisey, and R. J. Colton. 1994a. Direct measurement of the forces between complementary strands of DNA. *Science.* 266: 771–773.

Lee, G. U., D. A. Kidwell, and R. J. Colton. 1994b. Sensing discrete streptavidin-biotin interactions with atomic force microscopy. *Langmuir.* 10:354–357.

Low, B. W., W. W. Fullerton, and L. S. Rosen. 1974. Insulin/proinsulin, a new crystalline complex. *Nature.* 248:339–340.

Malkin, A. J., T. J. Land, Y. G. Kuznetsov, A. McPherson, and J. J. De Yoreo. 1995. Investigation of virus crystal growth mechanisms by in-situ atomic force microscopy. *Phys. Rev. Lett.* 75:2778–2781.

Markman, O., D. Elias, L. Addadi, I. R. Cohen, and Z. Berkovitch-Yellin. 1992. Monoclonal antibodies to insulin and to the insulin receptor (anti-ID) modify the morphologies of insulin crystals. *J. Crystal Growth.* 122:344–350.

Matthews, B. W. 1968. Solvent content of protein crystals. *J. Mol. Biol.* 33:491–497.

Milthorpe, B. K., L. W. Nichol, and P. D. Jeffrey. 1977. The polymerization pattern of zinc(II)-insulin at pH 7.0. *Biochim. Biophys. Acta.* 495:195–202.

Moy, V. T., E-L. Florin, and H. E. Gaub. 1994. Adhesive forces between ligand and receptor measured by AFM. *Colloids Surfaces A.* 93:343–348.

Noever, D. A. 1995a. Kinetic effects in protein crystals. I. The role of hydration in protein aggregation. *J. Phys. D. Appl. Phys.* 28:1384–1392.

Noever, D. A. 1995b. Kinetic effects in protein crystals. II. Geometry and misalignment tolerance with experimental results. *J. Phys. D. Appl. Phys.* 28:1393–1399.

Ohnesorge, F., W. M. Heckl, W. Haeberle, D. Pum, M. Sara, H. Schindler, K. Schilcher, A. Kiener, D. P. E. Smith, U. B. Sleytr, and G. Binnig. 1992. Scanning force microscopy studies of the S-layers from Bacillus coagulans E38–66, Bacillus sphaericus CCM2177 and of an antibody binding process. *Ultramicroscopy.* 42–44:1236–1242.

Oosawa, F., and M. Kasai. 1962. A theory of linear and helical aggregations of macromolecules. *J. Mol. Biol.* 4:10–21.

Pederson, J. S., S. Hansen, and R. Bauer. 1994. The aggregation behavior of zinc-free insulin studied by small-angle neutron scattering. *Eur. Biophys. J.* 22:379–389.

Pusey, M. L. 1991. Estimation of the initial equilibrium constants in the formation of tetragonal lysozyme nuclei. *J. Crystal Growth.* 110:60–65.

Radmacher, M., M. Fritz, J. P. Cleveland, D. R. Walters, and P. K. Hansma. 1994. Imaging adhesion forces and elasticity of lysozyme adsorbed on mica by atomic force microscopy. *Langmuir.* 10:3809–3814.

Sazaki, G., H. Ooshima, J. Kato, Y. Harano, and N. Hirokaw. 1993. Mechanism of crystallization of enzyme protein thermolysin. *J. Crystal Growth.* 130:357–367.

Smith, G. D., and E. Ciszak. 1994. The structure of a complex of hexameric insulin and 4′-hydroxyacetanilide. *Proc. Natl. Acad. Sci. USA.* 91: 8851–8855.

Smith, G. D., and G. G. Dodson. 1992. Structure of a rhombohedral R_6 insulin/phenol complex. *Proteins.* 14:401–408.

Smith, G. D., D. C. Swenson, E. J. Dodson, G. G. Dodson, and C. D. Reynolds. 1984. Structural stability in the 4-zinc human insulin hexamer. *Proc. Natl. Acad. Sci. USA.* 81:7093–7097.

Söhnel, O. 1982. Electrolyte crystal-aqueous solution interfacial tensions from crystallization data. *J. Crystal Growth.* 57:101–108.

Thibault, F., J. Langowski, and R. Leverman. 1992. Optimizing protein crystallization by aggregate size distribution analysis using dynamic light scattering. *J. Crystal Growth.* 122:50–59.

Weisenhorn, A. L., F.-J. Schmitt, W. Knoll, and P. K. Hansma. 1992. Streptavidian binding observed with an atomic force microscope. *Ultramicroscopy.* 42–44:1125–1132.

Wilson, A. J. C., editor. 1992. International Tables for Crystallography. Vol. C: Mathematical/Physical/Chemical Tables. Kluwer Academic Publishers, Dordrecht, The Netherlands.

Wilson, L. J., and M. L. Pusey. 1992. Determination of monomer concentrations in crystallizing lysozyme solutions. *J. Crystal Growth.* 122:8–13.